N_2 monolayer and bilayer adsorbed on Ag(110) at 15 K: Structure and orientational ordering

C. Ramseyer and C. Girardet
Laboratoire de Physique Moléculaire, UMR CNRS 6624, Faculté des Sciences La Bouloie, Université de Franche-Comté, 25030 Besançon Cedex, France

F. Bartolucci, G. Schmitz, and R. Franchy
Institut für Grenzflächenforschung und Vakuumphysik, KFA-Forschungszentrum Jülich, D-52425 Jülich, Germany

D. Teillet-Billy and J. P. Gauyacq
Laboratoire des Collisions Atomiques et Moléculaires, UMR CNRS 281, Université de Paris Sud, Batiment 351, 91405 Orsay, France
(Received 21 January 1998; revised manuscript received 25 March 1998)

The growth and the structure of an N_2 monolayer and bilayer physisorbed on Ag(110) at 15 K were investigated by means of thermal desorption spectroscopy and low-energy electron diffraction (LEED) and compared with structures determined from interaction potential calculations. The N_2 monolayer desorbs at 40 K with a desorption energy of 104 ± 1 meV while the bilayer desorbs at 32 K with an energy of 73 ± 1 meV. The LEED pattern of the monolayer corresponds to a parallelogram structure. For the bilayer a hexagonal structure was found. An energy minimization procedure based on simulated annealing algorithm gives adsorption energy values very consistent with the experimental data for the monolayer and bilayer. It shows, furthermore, that the monolayer geometry corresponds to a herringbone high-order commensurate phase while the second layer displays two isoenergetical structures: a relatively dilute herringbone phase and a dense hexagonal four-sublattice pinwheel structure. This latter structure has the symmetry observed in the LEED pattern. [S0163-1829(98)00231-8]

I. INTRODUCTION

The structural arrangement of adspecies[1] has been extensively studied for rare gas atoms physisorbed on a variety of hexagonal,[2–4] square,[5,6] and rectangular[7–9] substrates. The next step towards more complex systems was to investigate the adsorption of nonspherical adsorbates, since in addition to the translational ordering of the molecular centers of mass, the orientation of the molecular axes comes into play. The orientation ordering can give rise to complex structures leading to herringbone or pinwheel molecular arrangements and to new types of phase diagrams.[10] In recent decades, people concentrated particularly on the superstructures formed by diatomic molecules (N_2,CO) adsorbed on relatively smooth surfaces.[11] It was shown that the N_2 quadrupole moment plays a crucial role through the lateral interactions in determining major parts of the phase diagram and the corresponding phase transitions vs temperature and coverage.

The adsorption of N_2 on graphite[1] is known to be a model system due to its relative simplicity and to the extensive information provided by twenty years of investigation from both experimental and theoretical studies. Due to the tremendous amount of data, there is a broad consensus about the interpretation of the phase diagram obtained at different N_2 coverages. At low temperature and in the monolayer regime, low-energy electron diffraction (LEED) (Refs. 12–15) and neutron diffraction patterns[16] show the occurrence of a commensurate lattice that may be compressed to a uniaxial incommensurate herringbone lattice. Under further compression N_2 may form nonplanar herringbone geometries or pinwheel structures depending on the N_2 coverage and thus on the magnitude of the lateral interactions. Similar herringbone phases were evidenced by LEED and neutron scattering experiments for CO adsorbed on graphite[17] and expected from thermodynamics and potential calculations for CO and N_2 on boron nitride.[18] These experimental features were corroborated by numerical approaches including energy minimization at 0 K based on realistic interaction potentials,[19] Monte Carlo methods[20] and molecular dynamics simulations.[21,22]

The adsorption of N_2 on triangular surfaces such as Ag(111) has been very recently investigated using LEED experiments.[23] The results indicated that at coverages up to the saturated monolayer, N_2 (like CO) forms a rotated incommensurate hexagonal structure, while no additional order was noted upon adsorption of the second layer. The system N_2/Ag(111) was discussed in a general way using molecular-dynamics simulations from the low-temperature orientationally ordered solid to the melting of the solid by comparison with the results on graphite.[24]

Aside from the studies on hexagonal substrates, the anisotropic role of the corrugation was analyzed by considering the adsorption of N_2 on the rectangular Cu(110) substrate.[25,26] Thermal energy atom scattering (TEAS) experiments together with interaction potential calculations and molecular-dynamics simulations showed that this substrate exhibits troughs along the dense Cu rows, i.e., the $[1\bar{1}0]$ direction, in which the N_2 molecules were preferentially adsorbed. At low temperature (around 20 K), the monolayer forms a high-order commensurate phase with a large oval-shaped unit cell that contains seven N_2 molecules. The orientational ordering of the N_2 molecules obtained from calculations gives a seven-sublattice pinwheel structure.

In previous papers,[27,28] the formation of negative ion resonances (NIR's) of N_2 films adsorbed on Ag(110) at 15 K was investigated by high-resolution electron energy loss spectroscopy (EELS). Here, we study the growth and structure of the N_2 layers on the Ag(110) substrate at the same temperature by means of thermal desorption spectroscopy (TDS) and LEED. The experimental data are compared with energy calculations of the structure.

The paper is organized as follows: In Sec. II we describe the experimental conditions and we present the TDS and LEED results. Section III deals with the theoretical background of the interactions and the minimization procedure of the interaction potential. In Sec. IV we present the results of the calculations for the single admolecule, monolayer, and bilayer regimes. The experimental data are compared to the results of calculations and to other systems in Sec. V.

II. EXPERIMENTS

A. Experimental setup

The experiments were carried out in a UHV apparatus with a base pressure of about 5×10^{-11} mbar. The chamber is subdivided into two levels. The upper level is equipped with a cylindrical mirror analyzer (CMA) for Auger-electron spectroscopy, a three-grid LEED optic and a quadrupole mass spectrometer (QMS) for TDS. The computer-controlled EEL spectrometer[29] is based on 127° cylindrical deflectors and is mounted in the lower level of the UHV chamber. In the EELS experiment, the scattering plane was oriented perpendicular to the (110) surface and tilted 45° to the [001] direction, defined by the dense Ag rows of the Ag(110) substrate. For the TDS measurements the sample was positioned at 1 mm in the front of the aperture of the enclosure of the QMS. We used constant heating rates of 0.5–2.0 K/s that were controlled by a self-optimizing digital PID temperature controller. This controller generates temperature ramps (starting at 15 K) with an accuracy of about 0.1%.[30] The LEED study of the N_2 layers was taken at sample currents less than 10 nA in order to avoid desorption or dissociation of physisorbed nitrogen.[12] The sample of 8 mm diameter and 2.5 mm thickness is fixed on a continuous-flow cryostat and cooled with liquid helium to 15 K (cool-down time from 300 to 15 K less than 2 min). The crystal orientation has an accuracy of 0.1°. The sample is heated by electron impact and the temperature is measured using a NiCr/Ni thermocouple located at the back of the sample. The sample was cleaned via several cycles of Ar^+ ions sputtering (1 keV, 5 μA) at 300 K for 30 min followed by annealing at 800 K for 10 min. The clean Ag(110) surface exhibits a sharp (1×1) LEED pattern.

B. Results

1. TDS results

Figure 1 shows some typical TD spectra (time dependence of N_2 coverage θ vs temperature) taken for exposures between 0.1 and 20.0 L of N_2 adsorbed at 15 K. These spectra are measured in the temperature range between 15 and 300 K, with a heating rate of 0.5 K/s. The sample was annealed at 800 K for 3 min between each adsorption-desorption cycle. The partial pressures of the masses 28 (N_2) and 14 (N atoms) are detected simultaneously for each exposure. The temperature of the sample was calibrated using the known desorption energies of multilayers of Ar and N_2 (zeroth-order desorption).[31] For exposures less than 0.5 L, the TD spectra exhibit a small single desorption peak at 48 K that could be assigned to adsorption on defects. With increasing exposure from 0.5 up to 3.5 L a shoulder develops at 40 K that dominates the TD spectra for higher exposures. Then, the peak at 40 K saturates at an exposure of about 3.5 L. Since the integral of this peak corresponds to the coverage of 1 ML we calibrated the exposures in units of 1 ML (see the inset of Fig. 1).

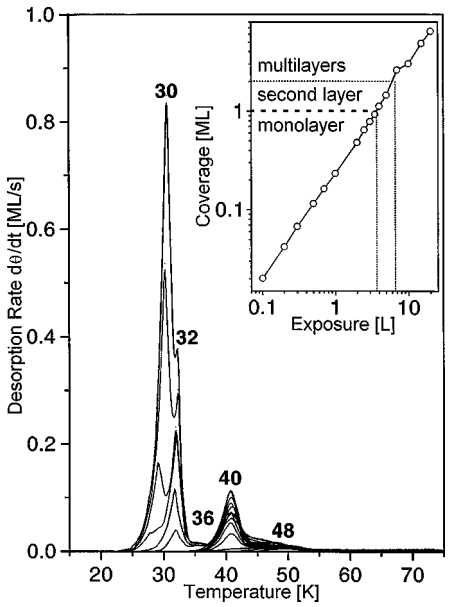

FIG. 1. TD spectra of mass 28 for exposures from 0.1 to 20.0 L of $^{14}N_2$ on Ag(110) at 15 K. The heating rate is 0.5 K/s and the partial pressure is calibrated to the desorption rate in ML/s. The inset shows the calibration of the exposure to units of 1 ML.

For exposures leading to coverages above 1 ML the TD spectra exhibit a second maximum located at 32 K, which corresponds to the desorption from the second layer. As expected this second layer saturates at about 7 L. For exposures above 8 L, desorption from the third and higher multilayers occurs, leading to the occurrence of a peak at 30 K. Finally, the TD spectrum corresponding to 20.0 L displays the distinct separation of the monolayer, second layer, and multilayer desorption. The desorption is a zero-order process for the multilayers and a first-order one for the monolayer. Thanks to the linearity of the temperature ramp, we are able to determine the activation energies of desorption at each coverage by a leading edge analysis (leading edge means less than 2% of a monolayer desorbed).[32] Figure 2 shows Arrhenius-plots [$\ln(d\theta/dt)$ vs $-1/T$] of the TD spectra. The inset shows the desorption energies of the monolayer, the second layer and the multilayers, respectively. The values of the desorption energies are 104 ± 1 meV for the monolayer, 73 ± 1 meV for the second layer, and 70 ± 1 meV for the multilayers. From the development of the desorption peaks it is obvious that the N_2 films are growing layer by layer.

2. LEED results

At 15 K, the clean Ag(110) surface exhibits exclusively a sharp (1×1) LEED pattern. The primitive unit cell of

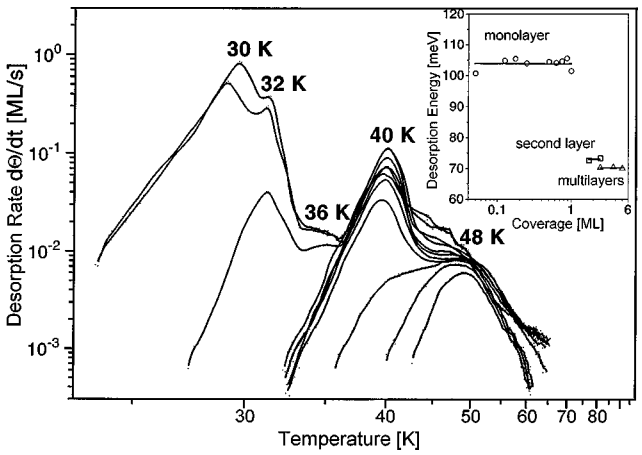

FIG. 2. Arrhenius plots $[\ln(d\theta/dt)$ vs $-1/T]$ of the TD spectra. The inset shows the desorption energies for the monolayer, bilayer, and multilayers calculated by a leading edge analysis.

Ag(110) has the lattice constants: $a_{S1}=2.89$ Å and $a_{S2}=4.09$ Å. Figure 3(a) (top) shows the LEED pattern of the N_2 monolayer adsorbed on Ag(110) at 15 K. Six spots appear in addition to the substrate spots: in fact, two spots are superimposed with the substrate reflexes and only four are separately seen. The scheme of the LEED spots is shown at the bottom of Fig. 3(a), where a_{S1}^* and a_{S2}^* correspond to the reciprocal vectors of the Ag(110) substrate while a_1^* and a_2^* are the reciprocal lattice vectors of the N_2 monolayer. Based on the LEED pattern, we propose a unit cell for the real-space structure, having a parallelogram shape with the lattice parameters $a_1=3.85$ Å, $a_2=4.34$ Å and $\gamma=70.5°$. The mean area per nitrogen molecule in the monolayer is 15.74 Å^2. Figure 3(b) (top) shows the LEED pattern of the second layer of N_2. The six observed spots have a hexagonal symmetry, and they are slightly elongated along the tangential direction. From the LEED pattern, we determine that the unit cell in the real space is hexagonal with $b=b_1=b_2=4.02$ Å,

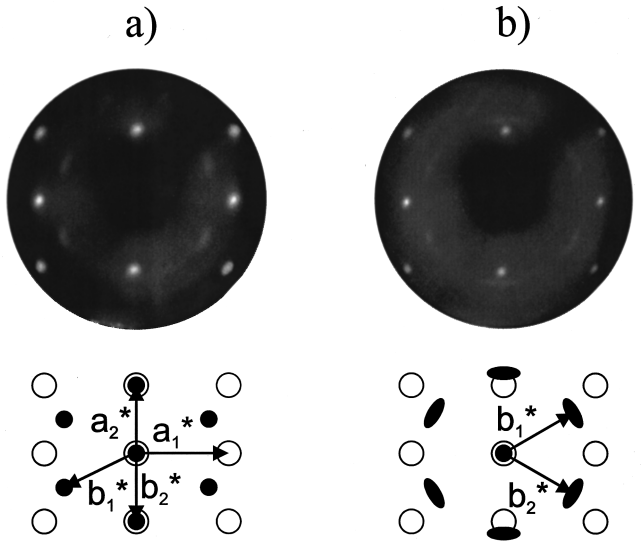

FIG. 3. LEED pattern at a primary energy of 66 eV: (a) for 1 ML N_2 and (b) for the bilayer N_2 on Ag(110) at 15 K. Below each LEED pattern are schemes with the reciprocal lattice vectors a_1^*, a_2^* (of the substrate) and b_1^*, b_2^* (of the overlayer).

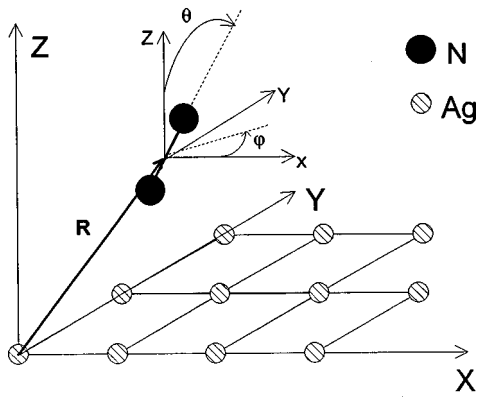

FIG. 4. Geometry of the Ag(110) surface with the N_2 admolecule. The substrate is described by a rectangular unit cell of area (2.89×4.09) Å^2. The position of the center of mass of the molecule is referred to an absolute frame (X,Y,Z) by the vector $\mathbf{R}$ and the molecule orientation by the Euler angles $\mathbf{\Omega}=(\varphi,\theta)$.

and the mean area per nitrogen molecule (14.0 Å^2) in the second layer is significantly smaller than in the monolayer. Note that we used an electron energy equal to 66 eV at low current (<10 nA) in order to not perturb the adsorbed structures. As a result higher-order diffraction peaks that could provide additional information on the layer geometry cannot be observed.

III. THEORETICAL BACKGROUND

A. Interaction potentials

The interaction potential $V(\mathbf{R},\mathbf{\Omega})$ for the N_2/Ag(110) system is the sum of an intralayer contribution V_{AA} and of an adsorbate-substrate term V_{AS}. It depends on the position $\mathbf{R}$ of the center of mass and on the orientation $\mathbf{\Omega}$ of the N_2 admolecule (Fig. 4). The dominant interactions in V_{AA} are the quantum dispersion-repulsion contributions supplemented by the electrostatic potential. For the quantum interactions, we use the usual pairwise Lennard-Jones (LJ) potential and for the electrostatic term, we choose a distributed charge description in order to include the effects of the finite extent of the molecules. V_{AA} can thus be written as

$$V_{AA}=\sum_{i,j}\sum_{p,q}\left(\sum_{k=6,12}4\epsilon_{ipjq}(-)^{k/2}\left(\frac{\sigma_{ipjq}}{r_{ipjq}}\right)^k+\frac{q_{ip}q_{jq}}{4\pi\epsilon_0 r_{ipjq}}\right), \tag{1}$$

where i and j label two nitrogen molecules and p and q are the interaction sites. For the LJ potential, the sites correspond to the center of mass of the N atoms. The set of parameters $(\epsilon_{N-N},\sigma_{N-N})$ for the various pairs are taken from the literature[33] and listed in Table I. For the electrostatic part of N_2, a three-point charges distribution model appears to be

TABLE I. Lennard-Jones parameters.

Atomic pairs	ε (meV)	σ (Å)
N-N[a]	3.14	3.318
N-Ag	4.227	3.486

[a]X1 model of Murthy *et al.* (Ref. 33).

convenient, with two charges equal to -0.405 a.u. at the nitrogen atom sites and one charge equal to $+0.810$ a.u. at the middle of the N-N bond.[33,34]

The adsorbate/substrate potential V_{AS} is mainly described by dispersion-repulsion interactions. Additional interactions known as substrate-mediated interactions and electrostatic image effects[35,36] are disregarded because they generally provide weak contributions to the adsorption energy and they did not change the equilibrium configuration of the adlayer. We describe V_{AS} by a LJ form similar to the one used for V_{AA} in Eq. (1), except that the sum is over the ip sites of the adsorbed molecules and jq is a single index that characterizes the substrate atoms. The choice of the LJ form is consistent with the expression used for a similar system, i.e., $N_2/Cu(110)$.[25,26] For this latter substrate, it was shown that such a potential can well account for the equilibrium[25,26,37] and the dynamical[38] properties of the N_2 or rare-gas layers. The LJ parameters $(\epsilon_{N-Ag}, \sigma_{N-Ag})$ listed in Table I reproduce the available equilibrium data taken from the thermal desorption and LEED experiments (Sec. II). In our calculations, we use the value of the adsorption energy equal to 80 meV. For the perpendicular frequency connected to the vibration of the adsorbate along the normal to the Ag surface a value of 3.7 meV seems reasonable by comparison with the measured value for N_2 on Cu(110).[39] The height of the nitrogen molecules above the surface is then about 3 Å. Other pairwise potentials have been proposed in the literature in order to explain the N_2 scattering from the (100) or (111) Ag surfaces. For instance, Tully and co-workers[40,41] used a Morse potential in place of the Lennard-Jones term because the repulsive part of this latter potential appeared to be too steep for explaining the collisional data.[42] However, its application to the present $N_2/Ag(110)$ system fails because it does not lead to a consistent value of the experimental adsorption energy. Note that the present LJ parameters have been applied to the $N_2/Ag(111)$ system and they appear to be successfully transferable to this system.

B. Minimization procedure

The determination of the equilibrium geometry of the adsorbed molecules is obtained by minimizing the total potential $V = V_{AA} + V_{AS}$ with respect to the $5N$ variables which characterize the N molecules lying on the Ag(110) substrate. Each molecule has three translational (X,Y,Z) and two rotational (φ,θ) degrees of freedom connected, respectively, to the position $\mathbf{R}$ of its center of mass and to the orientation $\mathbf{\Omega}$ of its molecular axis. When N is sufficiently small $(N \leqslant 5)$ a conventional numerical gradient procedure is used and we reach rapidly the absolute minimum of V. For larger N values, the number of local minima increases drastically and the gradient procedure obviously fails. When the adlayer is commensurate with the substrate, one can take advantage of the resulting periodicity and optimize the variables connected to the molecules that belong to the unit cell, only. When it is not the case or when the number of molecules contained in this cell is still too large $(N \geqslant 5)$ then statistical approaches are more convenient.

Simulated annealing (SA) is one of these methods that was developed to optimize such systems.[43,44] The basic idea is close to the physical annealing scheme applied to crystal growth in the sense that low temperature is not a sufficient condition for finding the optimized ground state of matter, and warming then cooling very slowly the matter will result in a much better ordered sample. The SA process consists of first melting the system being optimized at a high effective temperature, then lowering the temperature by slow stages until the system freezes and no further changes occur. At each temperature, the simulation must proceed long enough for the system to reach a steady state. Inside each step of temperature, a Metropolis algorithm is used. In such an algorithm, a degree of freedom is given a small random displacement and the resulting energy change ΔE is calculated. When $\Delta E \leqslant 0$, the displacement is accepted, and the displaced configuration is used as the starting point of the next step. In the case $\Delta E \geqslant 0$, the probability that the configuration is accepted is determined by the Boltzmann distribution at temperature T, $P(\Delta E) = \exp(-\Delta E/kT)$. If $P(\Delta E)$ is larger than a random number uniformly distributed in the interval $(0,1)$, then the configuration is accepted; if not, it is rejected and the original configuration is used to start the next step. By repeating this basic scheme many times, we simulate the thermal motions of a system in equilibrium with a heat bath at temperature T.

It should be mentioned here that SA differs from other conventional optimization techniques in that the absolute minimum search procedure cannot be trapped into a metastable state since transitions out of a local minimum are always possible at finite temperature. A second important feature is the ''divide-and-conquer'' strategy of the SA algorithm.[43] Gross features of the eventual state of the system appear at higher temperatures while fine details develop at lower temperatures.

To solve a peculiar optimization problem by simulated annealing, several parameters have to be chosen. Firstly, there are generic decisions, usually denominated as the cooling scheme, which are common to any SA implementation problems. The following parameters must be specified to define the annealing strategy: the initial (T_i) and final (T_f) values of temperature, and the rule for decreasing temperature. Among the tremendous temperature-quenching schemes that are given in the literature,[45] we chose the most common one according to Kirkpatrick,[43]

$$T_{n+1} = \alpha T_n . \tag{2}$$

The quenching factor α determines the rate of temperature drop between two consecutive steps in the SA algorithm. It is thus directly connected to the number of iterations that are required to ensure the accuracy of the method. When α is close to zero, then the temperature jumps are too large and the system will freeze in a metastable state. In contrast when α is close to 1, the system should undoubtedly reach the absolute minimum of the potential energy, but with the counterpart that the CPU time drastically increases. Note that this decreasing rule is consistent with the physical annealing process in the sense that there are large temperature jumps at high temperature and very small jumps at lower temperature. The values of the parameters α, T_i, and T_f, in this particular case, are equal to 0.8, 500 K, and 10^{-12} K in order to be sure that we reached the absolute minimum. It should be noted that the temperature occurring in the SA algorithm is a

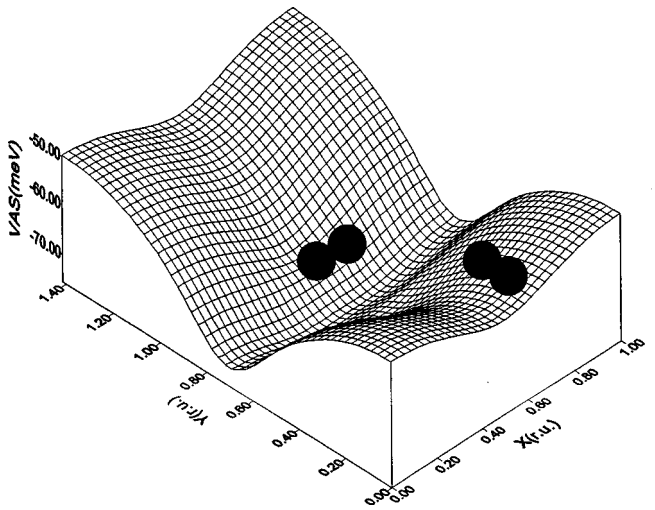

FIG. 5. Potential-energy map (energy in meV) for a single N_2 admolecule adsorbed on the Ag(110) surface. The rectangle corresponds to the unit cell of Ag(110). The lateral positions X and Y of the N_2 center of mass axis are given in reduced units, with respect to the lattice constant $a_S = 2.89$ Å.

control parameter, only, and that it should not be confused with the physical temperature.

Secondly, there are specific decisions that are closely related to the system to be solved. Indeed, the efficiency of the SA calculations depends crucially on the way the neighboring configurations are generated. In practice, several empirical attempts have to be made in order to find the appropriate conditions. For instance, while, in principle, the absolute minimum can be reached from any initial configuration of the admolecules, this latter one is chosen very carefully in order to minimize the CPU time. This time increases significantly when nonrealistic starting configurations are considered. Moreover, the number of neighboring configurations must be sufficiently large to represent the thermal equilibrium of the molecules at temperature T and sufficiently small to optimize the running time of the SA algorithm. All these specific decisions will be discussed in the numerical part (Sec. IV).

IV. NUMERICAL RESULTS

A. Equilibrium geometries

1. Single admolecule

A preliminary analysis of the interaction potential between a single N_2 molecule and the Ag(110) substrate gives information on the holding contribution and on the corrugation experienced by the admolecule. Figure 5 displays the potential-energy map experienced by the molecule that moves above the surface. This map was obtained with the help of a numerical gradient technique by minimizing the holding potential V_{AS} with respect to the perpendicular translation of the center of mass of the N_2 molecule and to the molecule orientation. The most stable adsorption site is found at the center of the rectangular unit cell (hollow site) of Ag(110) with an adsorption energy equal to 76 meV, at a height of 3.0 Å. The substrate is significantly anisotropic with large energy differences along the crystallographic directions. Along the [001] direction (**Y** axis) parallel to the dense Ag rows the corrugation can reach 20 meV while it is only 6 meV in the $[1\bar{1}0]$ direction (**X** axis). The N_2 molecule lies into potential troughs parallel to the dense Ag rows and it is adsorbed flat on the equilibrium site ($\theta = 90°$). Its axis is slightly tilted ($\theta \simeq 70°$) when it is adsorbed above the dense Ag rows. A similar feature is obtained for the azimuthal angle φ since the molecule is always parallel to the dense Ag rows ($\varphi = 0°$) except above them where it becomes perpendicular ($\varphi = 90°$) to the rows. The behavior of this peculiar orientational ordering is mainly due to the corrugation experienced by the N_2 molecule that is large enough inside the troughs to hinder the polar and azimuthal rotations of the molecular axis.

2. Monolayer geometry

Then the SA minimization procedure was applied to find the most stable structure for the zN_2 monolayer. Since we have no obvious information regarding the commensurability of the monolayer with the substrate, we considered a set of 70 N_2 molecules schematizing the layer in order to be free of side effects. Two initial configurations were investigated that correspond in fact to two asymptotic situations: The first one for an uncorrugated surface and the second for a highly corrugated substrate. In the first configuration, the initial positions of the molecules are taken to be those of the (111) plane of the fcc bulk N_2 solid, namely, they are arranged according to regular triangles with each side equal to 4.0 Å. For the orientations of the molecules a random distribution was chosen. In the second configuration, we assume that all of the molecules lie in the troughs with their axes flat and parallel to the $[1\bar{1}0]$ direction ($\varphi = 0°$), in order to accomodate the rectangular shape of the Ag(110) surface.

The minimization procedure starting from these two configurations converges toward the same stable structure represented in Fig. 6(a). Regarding the poor periodicity of the structure, we can say that N_2 forms either a high-order commensurate or an incommensurate phase with Ag(110). Because of the large corrugation along **Y**, the N_2 molecules still lie in the troughs since the molecule-surface distance is constant and equal to 3.0 Å. The average energy per molecule, equal to 96 meV, can be separated into a large holding contribution (76 meV) and a small lateral contribution (20 meV). This latter value seems reasonable since in the bulk nitrogen lattice the lateral energy does not exceed 30 meV. The final distribution of the molecular centers of mass and orientations is drawn in Figs. 6(b)–6(d). Figure 6(b) clearly shows that the structure formed by the centers of mass is quasihexagonal. Indeed, one molecule is surrounded by six neighbors at the positions $\mathbf{R} = n_1\mathbf{a}_1 + n_2\mathbf{a}_2$ where n_1 and n_2 are integer numbers. $\mathbf{a}_1$ and $\mathbf{a}_2$ [Fig. 6(a)] define the primitive translation vectors of the unit cell connecting the N_2 centers of mass. Their lenghts a_1 and a_2 are equal to 3.9 Å and 4.4 Å, respectively, leading to an average area of 16 $Å^2$ per molecule. As a consequence, each peak occurring in Fig. 6(b) defines a particular distance R with a standard deviation of about 0.3 Å. The second peak around 4.4 Å has an intensity twice as large as the first peak because each N_2 molecule has four nearest neighbors located in adjacent rows at a distance a_2 and two neighbors in the same row at a distance a_1.

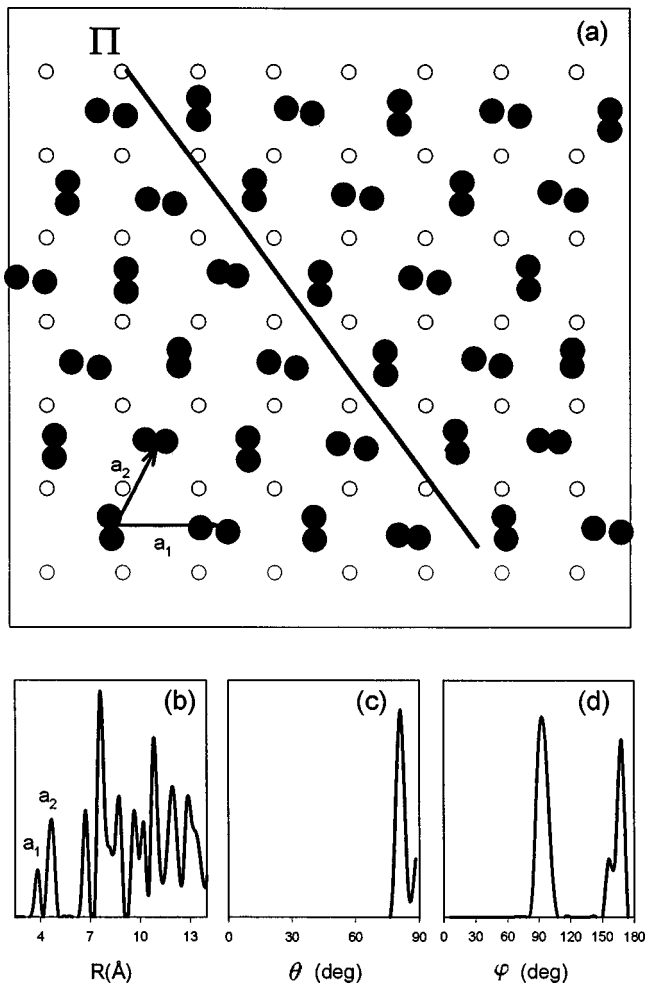

FIG. 6. N_2 monolayer geometry adsorbed on Ag(110). (a) Top view of the molecules (black circles) adsorbed on the rectangular lattice Ag(110) (white circles) showing the herringbone structure characterized by the glide plane Π. $\mathbf{a}_1$ and $\mathbf{a}_2$ define the vectors of the unit cell restricting to the centers of mass of the N_2 molecules. Distribution of the centers of mass (b), polar angles θ (c) and azimuthal angles φ (d) determined from the simulated annealing method.

The second-nearest neighbors are then at distances $a_1\sqrt{3}$ and $a_2\sqrt{3}$ (respectively, 6.8 and 7.6 Å). Figure 6(c) shows that the molecules remain nearly flat on the surface since a single peak is obtained at $\theta=80°$ with a standard deviation of 10°. Two typical values occur for the azimuthal angles φ, at 90° and 170° [Fig. 6(d)]. These results indicate that the monolayer structure can be considered as a ''two-in'' herringbone structure where two types of molecules that are nearly perpendicular to each other ($170°-90°=80°$) coexist on the surface. The occurrence of such a preferential orientation for this herringbone structure was not obvious at all, since the glide plane Π and its perpendicular homolog [not represented on Fig. 6(a)] for this structure do not follow a preferential crystallographic direction of the substrate but, rather, result from a subtle competition between the holding and the lateral interactions.

3. Bilayer geometry

We have investigated the structure of the bilayer by the same SA technique. The potential energies of both the bilayer and the monolayer are minimized simultaneously since, in principle, this latter could change its equilibrium geometry when a second N_2 layer lies above it. We chose the herringbone phase obtained previously to be the starting configuration of the first layer. For the second layer, a hexagonal phase where the nearest-neighbor molecules are separated by 4 Å was expected to be a reliable structure, close to the bulk nitrogen lattice.

The results of calculations show that the monolayer still forms a quasihexagonal two-dimensional lattice but it is slightly distorted as indicated by the small change of the primitive vector lengths ($a_1=3.9$ Å and $a_2=4.2$ Å). Nevertheless, the average energy per molecule equal to 95.8 meV, is very close to the single-monolayer value. All of the molecules are now perfectly flat on the surface ($\theta=90°$), as if the second layer acted as a ''press'' on the first layer. The values of the azimuthal angle do not change ($\varphi=90°$ and 170°), indicating that the large substrate corrugation along the **Y** direction hinders the molecular axes to rotate freely inside the potential trough.

For the bilayer, two structures are found to be stable at 0 K since they have the same potential energy per molecule (78.6 meV). The first structure [Fig. 7(a)]) appears as a dilute phase because each molecule occupies an average substrate area of 16 $Å^2$, only. In this phase, the molecules lie above the dense silver rows, at an average height of 6 Å above the surface. As shown in Fig. 7(b), the centers of mass of the molecules form a quasihexagonal structure with primitive translation vectors $\mathbf{b}_1$ and $\mathbf{b}_2$ having the lengths $b_1=4.1$ Å and $b_2=4.2$ Å. The orientations of the molecules are distributed in a large range of polar angles $60°\leqslant\theta\leqslant 90°$ [Fig. 7(c)] and this second layer does not show any azimuthal orientational ordering [Fig. 7(d)] in deep contrast with the monolayer structure. The second structure, represented in Fig. 8(a), is a more dense phase since the mean area per molecule decreases to 14.2 $Å^2$. Figure 8(b) shows that the centers of mass of the molecules are arranged according to a perfect hexagonal two-dimensional lattice with $b_1=b_2=4$ Å. As a result of this compact structure, the molecules form a pinwheel structure [Fig. 8(c)] with one upright molecule ($\theta=10°$) surrounded by six molecules lying nearly flat on the surface ($\theta=85°$). These flat molecules tend to coil around the pin molecule with successive azimuthal angles $\varphi=30°$, 90°, and 150°, thus forming a well-oriented structure [Figs. 8(a) and 8(d)]. Examination of Fig. 8(a) shows that the ratio between the flat and the pin molecules is about 3, which means that one flat molecule belongs in average to two wheels.

V. DISCUSSION

A. Comparison with experimental data

The energy per molecule in the monolayer deduced from TDS experiments is equal to 104 ± 1 meV. This value agrees quite well with the one calculated from our semiempirical potentials (96 meV). Moreover, the mean potential experienced by a molecule that belongs to the bilayer is calculated to be 78.6 meV and compares very well to the measured value of 74 ± 1 meV. This latter value is mostly a characteristic of the N_2-N_2 potential. We can consider that the very small deviations between the calculated and experimental values of the desorption energies for the first and second

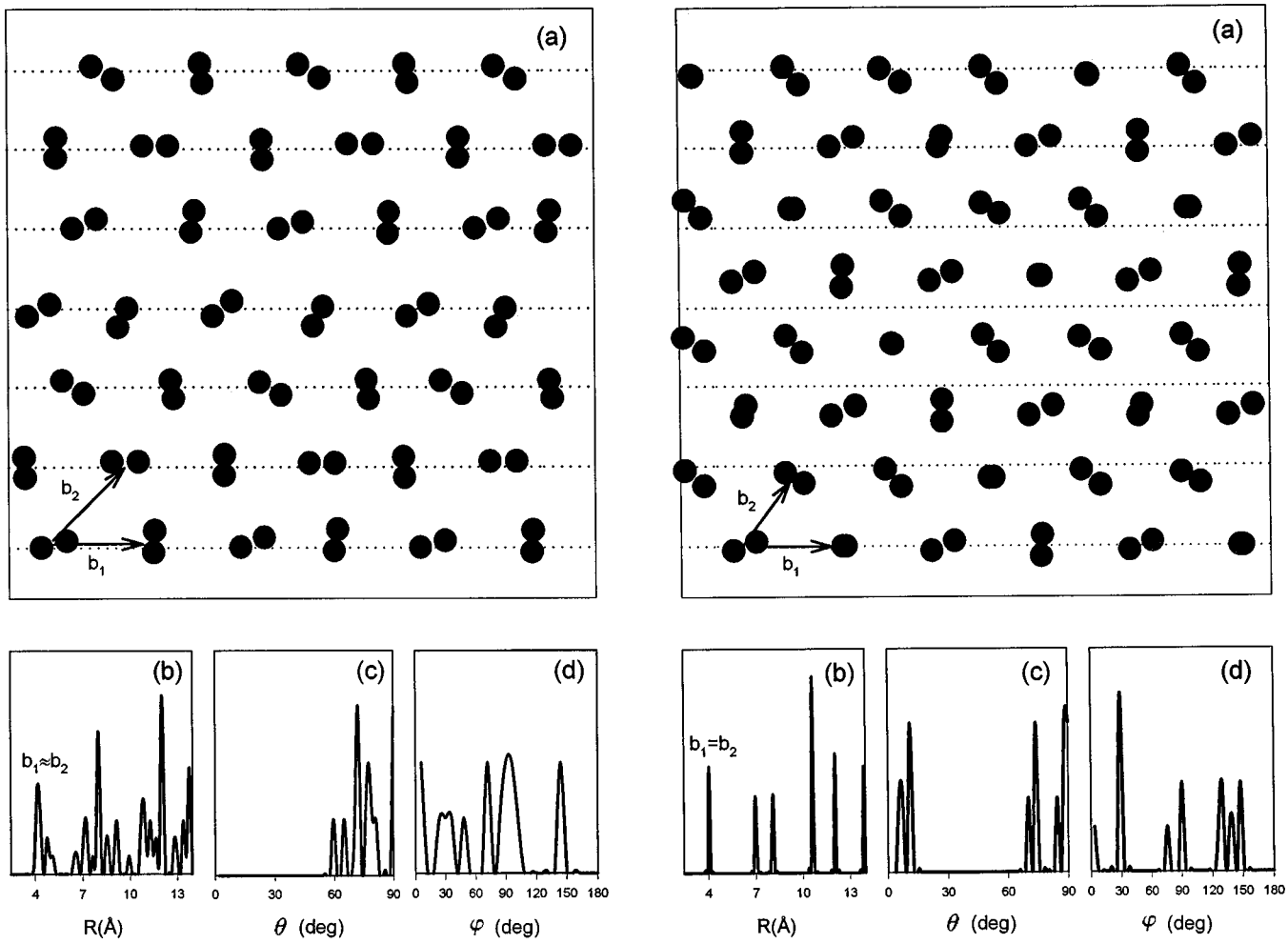

FIG. 7. Dilute phase of the N_2 bilayer adsorbed on Ag(110). (a) Top view of the molecules (black circles) adsorbed above the dense Ag rows (dotted lines). The monolayer is not represented in order to enlight the figure. $\mathbf{b}_1$ and $\mathbf{b}_2$ characterize the vectors of the unit cell connected to the centers of mass of the N_2 molecules. Distribution of the centers of mass (b), polar angles θ (c) and azimuthal angles φ (d) determined from the simulated annealing method.

FIG. 8. Dense phase of the N_2 bilayer adsorbed on Ag(110). (a) Top view of the molecules (black circles). The dotted lines refer to the dense Ag rows. The monolayer is not represented in order to enlight the figure. $\mathbf{b}_1$ and $\mathbf{b}_2$ characterize the vectors of the unit cell connected to the centers of mass of the N_2 molecules. Distribution of the centers of mass (b), polar angles θ (c) and azimuthal angles φ (d) determined from the simulated annealing method.

layers are a direct estimate of the accuracy of the adsorbate-substrate interactions. These slight differences could be due to disregarded interactions which represent about 10% of the total energy, i.e., within the margin of error occurring here. They could also come from an approximate interpretation of the experimental measurements since, in principle, the desorption energies in a nonequilibrium process should not directly be compared to the equilibrium potential values.

From the analysis of the LEED pattern at 15 K, the monolayer forms a quasihexagonal structure with lattice constants $a_1 = 3.85$ Å and $a_2 = 4.34$, Å where each molecule has an average area of 15.75 Å^2. The calculations show that the structure of the monolayer is incommensurate or highly commensurate with the underlying substrate. They corroborate fairly well these experimental features regarding the arrangement of the centers of mass of the molecules since in that case $a_1 = 3.9$ Å and $a_2 = 4.4$ Å. Moreover, the calculated structure of this adsorbed layer exhibits a herringbone phase with two perpendicular glide planes that do not coincide with preferential crystallographic directions of the substrate. These glide planes have not been evidenced from experiments and this could be a future goal for us to elucidate this point and to give additional information on the N_2 orientational ordering from the negative-ion resonance results.[27,46] However, in order to observe high-order diffraction peaks that could corroborate or invalidate their existence, higher electron energies are needed that certainly will affect the adsorbed layer.

Another theoretical result is the occurrence of two possible stable bilayer structures with different molecular densities. From the comparison with the LEED pattern, the dense phase, i.e., the hexagonal pinwheel geometry, seems to be the most reliable structure for the second layer. In experiments, the N_2 second layer is found to arrange in a perfect hexagonal lattice with $b_1 = b_2 = 4$ Å and an average area per molecule equal to 14 Å^2. The equilibrium geometry calculations show that the centers of mass of the molecules have exactly the same arrangement in this dense phase. Concerning the dilute phase, one question remains: whether this structure is metastable or, in contrast, observable at N_2 coverage less than 1 ML. At that time nothing concerning this

structure was found and further experiments at various temperatures should be of great help.

The results on the structure and on the adsorption energy for N_2/Ag(110) can be compared to the very recent LEED measurements[23] on the N_2/Ag(111) system. Indeed, for this triangular substrate, the monolayer heat of adsorption is equal to 103 ± 4 meV, very close to the value obtained on the rectangular surface, and the structure at 40 K is a rotated incommensurate hexagonal phase. In contrast, for the bilayer, the adsorption energy equal to 106 ± 6 meV is appreciably larger for the triangular than for the rectangular surface (79 meV). Moreover, the bilayer on Ag(111) does not exhibit order, in contrast with the pinwheel structure formed on Ag(110), due probably to the smaller corrugation on the dense (111) face. Such a large energy for the second N_2 layer is quite surprising when compared to our results on Ag(110) and to values on graphite, these two latter values being consistent.

B. Comparison with other systems

Nineteen years ago, Harris and Berlinsky, and later Mouritsen and Berlinsky, used a mean-field theory[10] to study the orientational ordering of H_2 and D_2 molecules on the basal plane of grafoil. The molecules experienced, on one hand, mutual interactions through the electrostatic quadrupole-quadrupole contribution only, and, on the other hand, the homogeneous crystal field due to the substrate leading to the holding potential V_C. A generic phase diagram was obtained for which four distinct orientationally ordered phases were shown to occur, depending on the temperature and the relative strength of the holding potential V_C and of the quadrupolar coupling constant $\Gamma(\Gamma\geqslant 0)$. In the ''two-in'' herringbone phase stable for large negative values of V_C, the molecules were flat above the surface ($\theta=90°$) with two possible in-plane orientations. In the ''two-out'' phase, the molecules still formed a two-sublattice herringbone structure, but the molecular axes were tilted with respect to the surface plane. At smaller but still negative V_C values, a four-sublattice pinwheel structure was obtained for which six molecules lying flat on the surface are coiled around a pin molecule. Finally, for positive V_C values, a ferrorotational phase was obtained with a single tilted molecule per unit cell.

In order to corroborate (or invalidate) these mean-field results for classical molecules, a large number of experiments[11] were devoted to molecular nitrogen adsorbed on the (0001) basal plane of graphite. A well-known particularity of this hexagonal substate is the generally small corrugation (a few meV, only) experienced by small linear admolecules such as N_2 and CO. Three of the four predicted structures were elucidated.[10] LEED experiments[12–14] corroborated by neutron diffraction results[16] showed the occurrence of commensurate in-plane and out-of-plane herringbone geometries, depending on the N_2 coverage. Reinvestigation of the diffraction pattern for this system at monolayer completion revealed[15] that the signals assigned to the compressed out-of-plane herringbone structure could also be interpreted in terms of a four-sublattice pinwheel structure. Similar herringbone phases were found for CO adsorbed on graphite[17] from LEED and neutron signals and from thermodynamic results for CO and N_2 adsorbed on the hexagonal plane of BN.[18] Different numerical approaches including energy minimization based on realistic potentials,[19] Monte Carlo methods,[20] and molecular dynamics simulations[21,22] were performed on the N_2/graphite system, and all support the existence of the compressed herringbone phases and of a pinwheel phase at monolayer completion.

Beside the studies on graphite and BN substrates, a different situation connected to the anisotropic role of the corrugation was analyzed when considering the N_2 adsorption on the rectangular Cu(110) substrate.[25,26] Thermal helium atom scattering experiments together with interaction potential calculations and molecular-dynamics simulations revealed that, in the monolayer regime, the N_2 molecules remain inside the unidirectional troughs formed by the dense Cu rows of the substrate. These molecules arrange in a quite complex high-order commensurate phase with a large quasi-hexagonal unit cell. This latter one contains seven N_2 molecules arranged in a seven-sublattice pinwheel structure. In that case, the application of the mean-field theory would lead to a ratio $|V_C/\Gamma|$ equal to 2. This value should favor the occurrence of either a pinwheel or a two-out herringbone structure. In the bilayer, the molecules were arranged in a slightly distorted hexagonal structure, but neither the experimental data nor the theoretical investigations succeeded in determining the orientational ordering of the molecules.

In light of these results, we see that the N_2/Ag(110) system should behave as an intermediate system between nitrogen adsorption on graphite and Cu(110). At monolayer completion, the large $|V_C/\Gamma|$ ratio, equal to about 4, could explain why the nitrogen molecules are flat on the Ag surface and form a two-in herringbone structure. Moreover, the anisotropic Ag surface tends to constrain the molecules to stay inside the troughs along the X direction. As a result, a glide plane with a specific orientation that does not coincide with the crystallographic directions of the substrate is found. In contrast, in the second N_2 layer, the influence of the interactions with the substrate decreases substantially, leading to a value of $|V_C/\Gamma|$ equal to 1.5. In this case, the nitrogen molecules can form either a two-out herringbone structure (dilute phase) or a pinwheel structure (dense phase) depending on the coverage rate and on the temperature range, in very close agreement with our present calculations.

VI. CONCLUSION

In this paper, we have shown that semiempirical interaction potentials can accurately interpret the values of the desorption energies issued from TDS experiments and the layer structures given by the LEED patterns, for the N_2/Ag(110) system. At this step, the calculations provide more information, especially on the molecule orientations above the surface, than the one given by LEED. Resonance electron scattering has been shown[47] to be an efficient probe of the molecule orientation when the observed angular distributions are compared to the calculated distributions. The knowledge of the resonance symmetry of the isolated N_2 molecule and of the structure of the layers, together with the selection rules for the angular profile, should predict whether a molecule stands flat or upright above the surface. Negative ion reso-

nances have been experimentally investigated[27] for the N_2/Ag(110) system and a combination of angular distribution calculations based on the layer structure determined in this paper and of the electronic angular emission profile of N_2 will be discussed in a companion paper[46] to test the accuracy of the angle dependence of the interaction potentials.

ACKNOWLEDGMENTS

The authors would like to thank L. W. Bruch for a prepublication copy of his work on N_2 adsorbed on Ag(111) and for fruitful discussions. This work was partially supported by the Human Capital and Mobility program of the European Community under Contract No. CHRX-CT93-0326.

[1] L. W. Bruch, M. W. Cole, and E. Zaremba, *Physical Adsorption: Forces and Phenomena* (Clarendon Press, Oxford, 1997).
[2] J. Unguris, L. W. Bruch, and M. B. Webb, Surf. Sci. **87**, 522 (1979); **114**, 219 (1982).
[3] E. D. Specht, A. Mak, C. Peters, M. Sutton, R. J. Birgeneau, K. L. D'Amico, D. E. Moncton, S. E. Nagler, and P. M. Horn, Z. Phys. B **69**, 347 (1988).
[4] K. Kern and G. Comsa, in *Phase Transitions in Surface Films 2*, edited by H. Taub *et al.* (Plenum, New York, 1991), p. 41.
[5] T. Meichel, J. Suzanne, C. Girard, and C. Girardet, Phys. Rev. B **38**, 3781 (1988).
[6] M. F. M. De Kieviet, D. Bahatt, G. Scoles, G. Vidali, and M. Karimi, Surf. Sci. **365**, 789 (1996).
[7] A. Glachant, M. Jaubert, M. Bienfait, and G. Boato, Surf. Sci. **115**, 219 (1981).
[8] W. Berndt, Surf. Sci. **219**, 161 (1989).
[9] P. Zeppenfeld, M. Büchel, J. George, R. David, G. Comsa, C. Ramseyer, and C. Girardet, Surf. Sci. **366**, 1 (1996).
[10] A. B. Harris and A. J. Berlinsky, Can. J. Phys. **57**, 1852 (1979); O. G. Mouritsen and A. J. Berlinsky, Phys. Rev. Lett. **48**, 181 (1982).
[11] For a recent review, see D. Marx and H. Wiechert, in *Advances in Chemical Physics*, edited by I. Progogine and S. A. Rice (Wiley, New York, 1996), Vol. 95, p. 213.
[12] R. D. Diehl, M. F. Toney, and S. C. Fain, Jr., Phys. Rev. Lett. **48**, 177 (1982).
[13] R. D. Diehl and S. C. Fain, Jr., Surf. Sci. **125**, 116 (1983).
[14] H. You and S. C. Fain, Jr., Faraday Discuss. Chem. Soc. **80**, 159 (1985).
[15] S.-K. Wang, J. C. Newton, R. Wang, H. Taub, J. R. Dennison, and H. Shechter, Phys. Rev. B **39**, 10 331 (1989).
[16] R. Wang, S.-K. Wang, H. Taub, J. C. Newton, and H. Shechter, Phys. Rev. B **35**, 5841 (1987).
[17] H. You and S. C. Fain, Jr., Surf. Sci. **151**, 361 (1985).
[18] W. Li, P. Shrestha, A. D. Migone, A. Marmier, and C. Girardet, Phys. Rev. B **54**, 8833 (1996).
[19] L. W. Bruch, J. Chem. Phys. **79**, 3148 (1983).
[20] B. Kuchta and R. D. Etters, Phys. Rev. B **36**, 3400 (1987); J. Chem. Phys. **88**, 2793 (1988).
[21] J. Talbot, D. J. Tildesley, and W. A. Steele, Mol. Phys. **51**, 1331 (1984).
[22] V. R. Bhethanabotla and W. A. Steele, J. Chem. Phys. **91**, 4346 (1989).
[23] G. S. Leatherman and R. D. Diehl, Langmuir **13**, 7063 (1997).
[24] L. W. Bruch and F. Y. Hansen, Phys. Rev. B **57**, 9285 (1998).
[25] P. Zeppenfeld, J. Goerge, V. Diercks, R. Halmer, R. David, G. Comsa, A. Marmier, C. Ramseyer, and C. Girardet, Phys. Rev. Lett. **78**, 1504 (1997).
[26] A. Marmier, C. Ramseyer, P. N. M. Hoang, C. Girardet, J. Goerge, P. Zeppenfeld, M. Büchel, R. David, and G. Comsa, Surf. Sci. **383**, 321 (1997).
[27] F. Bartolucci and R. Franchy, Surf. Sci. **368**, 27 (1996).
[28] R. Bartolucci, R. Franchy, J. A. M. C. Silva, A. M. C. Moutinho, D. Teillet-Billy, and H. P. Gauyacq, J. Chem. Phys. **108**, 2251 (1998).
[29] H. Ibach, *Electron Energy Loss Spectrometers, The Technology of High Performance*, Springer Series in Optical Sciences Vol. 63 (Springer-Verlag, Heidelberg, 1991).
[30] G. Schmitz, F. Bartolucci, P. Gassmann, and R. Franchy (unpublished).
[31] H. Schlichting and D. Menzel, Rev. Sci. Instrum. **64**, 2013 (1993).
[32] A. M. de Jong and J. W. Niemantsverdriet, Surf. Sci. **233**, 355 (1990).
[33] C. S. Murthy, K. Singer, M. L. Klein, and I. R. McDonald, Mol. Phys. **41**, 1382 (1980).
[34] A. J. Stone and M. Alderton, Mol. Phys. **56**, 1047 (1985).
[35] S. Rauber, J. P. Klein, M. W. Cole, and L. W. Bruch, Surf. Sci. **123**, 173 (1982).
[36] L. W. Bruch, Surf. Sci. **125**, 194 (1983).
[37] C. Ramseyer, C. Girardet, P. Zeppenfeld, J. Goerge, M. Büchel, and G. Comsa, Surf. Sci. **313**, 251 (1993).
[38] P. Zeppenfeld, M. Büchel, R. David, G. Comsa, C. Ramseyer, and C. Girardet, Phys. Rev. B **50**, 14 667 (1994); C. Ramseyer, V. Pouthier, C. Girardet, P. Zeppenfeld, M. Büchel, V. Diercks, and G. Comsa, *ibid.* **55**, 13 203 (1997).
[39] P. Zeppenfeld (private communication).
[40] C. W. Muhlhausen, J. Serry, J. C. Tully, G. E. Becker, and M. J. Cardillo, Isr. J. Chem. **22**, 315 (1982).
[41] A. C. Kummel, G. O. Sitz, R. N. Zare, and J. C. Tully, J. Chem. Phys. **89**, 6947 (1988).
[42] J. C. Tully, C. W. Muhlhausen, and L. R. Ruby, Ber. Bunsenges. Phys. Chem. **86**, 433 (1982).
[43] S. Kirckpatrick, C. D. Gelatt, Jr., and M. P. Vecchi, Science **220**, 671 (1983).
[44] V. Cerny, J. Optim. Theory Appl. **45**, 41 (1985).
[45] R. V. V. Vidal, *Applied Simulated Annealing*, Lectures Notes in Economics and Mathematics Systems, Vol. 396 (Springer, Berlin, 1993).
[46] D. Teillet-Billy, J. P. Gauyacq, F. Bartlucci, G. Schmitz, R. Franchy, C. Ramseyer, and C. Girardet (unpublished).
[47] K. M. Hock and R. E. Palmer, J. Chem. Phys. **97**, 8736 (1992).